Applied Chemical Engineering (2026) Volume 9 Issue 1 ISSN: 2578-2010 (O)
doi: 10.59429/ace.v9i1.5868

ORIGINAL RESEARCH ARTICLE

Deep learning and Multi-Sensor Remote Sensing for predicting Atlas cedar resilience: Integrating Landsat-8, Sentinel-2, and Field Inventories within an AI-Driven Ecological Monitoring Framework

Anass Legdou[1,*], Ayoub Souileh[2], Achraf Mabrouk[3], Said Lahssini[3], Bouchra Nassih[4], Aouatif Amine[1]

[1] *Advanced Systems Engineering Laboratory, ENSA Kenitra, Ibn Tofail University, Kenitra, 14000, Morocco*

[2] *L3GIE, Mohammadia Engineering School, Mohammed V University in Rabat, Rabat, 10090, Morocco*

[3] *National Forestry School of Engineers, Sale, 11000, Morocco*

[4] *Advanced Systems Engineering Laboratory, Faculty of Economics and Management, Ibn Tofail University, Kenitra, 14000, Morocco*

***Corresponding author:** Anass Legdou, anasslegdouseap@gmail.com

ARTICLE INFO

Received: 25 December 2025
Accepted: 26 January 2026
Available online: 06 February 2026

ABSTRACT

Atlas cedar (Cedrus atlantica) forests in Morocco's Middle Atlas are experiencing an accelerated decline due to combined climatic and human pressures. Building on previous work on forest transition modeling, this study presents a deep-learning–based framework designed to predict and monitor the ecological resilience of Atlas cedar ecosystems. Multi-sensor satellite images from Landsat-8 and Sentinel-2, combined with field inventory data from the Ain Leuh–Sidi M'Guild massif, were processed to evaluate vegetation health, canopy density, and regeneration potential from 2013 to 2024. A hybrid Convolutional Neural Network–Bidirectional Long Short-Term Memory (CNN–BiLSTM) model was built to capture both spatial and temporal patterns of forest loss and recovery.

Spectral indices such as NDVI, NBR, NDMI, and SAVI were extracted and standardized, while terrain features (altitude, slope, aspect) and bioclimatic variables (temperature seasonality, precipitation during the driest quarter) were included in the model. The hybrid CNN–BiLSTM architecture achieved an overall prediction accuracy of 94.7%, surpassing traditional machine learning methods (Random Forest, SVM, and Gradient Boosting). The spatio-temporal projections reveal a notable decline (−62%) of high-density cedar stands in low-elevation areas, while upper-slope refugia show partial stability and higher regeneration likelihoods.

These results demonstrate the potential of deep learning combined with high-resolution Earth observation data for real-time forest health monitoring and adaptive management. The developed framework provides an operational foundation for Morocco's Forest Strategy 2020–2030, enabling proactive decision-making for climate-resilient reforestation and ecological restoration in Mediterranean mountain ecosystems.

Keywords: Atlas cedar; deep learning; CNN–BiLSTM; Landsat-8 • Sentinel-2; forest resilience; climate change; remote sensing; Morocco; ecological forecasting

1. Introduction

Atlas cedar (*Cedrus atlantica*), an emblematic and endemic conifer of the western Mediterranean basin, constitutes a keystone species of Morocco's Middle Atlas Mountain ecosystems. These forests play a fundamental role in carbon storage[1]. soil conservation, biodiversity maintenance, and water regulation in semi-arid to sub-humid mountain environments[2]. However, over the past decades, Atlas cedar ecosystems have undergone a pronounced and accelerating decline, manifested by canopy dieback, reduced regeneration, and progressive replacement by oak coppices and degraded shrublands[3].

This degradation results from the combined and interacting effects of climate change and human pressure. On the one hand, rising temperatures, increased frequency and intensity of drought events, and longer dry seasons have imposed severe water stress on cedar stands, particularly at low and mid elevations. On the other hand, persistent anthropogenic disturbances such as overgrazing, fuelwood collection, soil trampling[4], and illegal logging have degraded soil structure, reduced regeneration capacity, and amplified ecosystem vulnerability. While human activities do not modify the regional climate itself, they strongly exacerbate the ecological impacts of climatic stress by weakening forest resilience and adaptive capacity, especially in environmentally marginal zones[5].

Monitoring and anticipating the spatio-temporal dynamics of forest degradation and resilience under these coupled pressures remains a major scientific and operational challenge. Traditional approaches based on forest inventories, although essential, are spatially discontinuous and difficult to update at the scale of large mountain massifs. In contrast, multi-sensor Earth observation data from platforms such as Landsat and Sentinel provide long-term, spatially explicit, and repetitive measurements of vegetation condition, canopy structure, and moisture stress, enabling continuous monitoring of forest ecosystems[6]. Over the last decade, numerous studies have relied on classical machine learning algorithms such as Random Forest (RF), Support Vector Machines (SVM), and Extreme Gradient Boosting (XGBoost) to model forest cover change, degradation patterns, and species distribution using remote sensing data. While these approaches have demonstrated good performance for static or quasi-static classification tasks, they suffer from important limitations when addressing forest resilience as a dynamic spatio-temporal process. In particular, these models generally (i) treat observations as independent in time, (ii) have limited ability to explicitly capture long-term temporal dependencies, and (iii) struggle to jointly exploit spatial context and temporal trajectories in multi-date satellite image series[7].

Recent advances in deep learning offer new perspectives for overcoming these limitations. Convolutional Neural Networks (CNNs) have proven highly efficient for extracting complex spatial patterns from high-dimensional imagery, while Recurrent Neural Networks (RNNs), and particularly Long Short-Term Memory (LSTM) architectures, are specifically designed to model temporal dependencies and sequential processes. The bidirectional variant (BiLSTM) further enhances this capability by learning temporal relationships both forward and backward in time, which is particularly relevant for ecological systems characterized by delayed responses, cumulative stress, and episodic recovery phases. The integration of CNN and BiLSTM architectures therefore provides a powerful framework for jointly modeling the spatial structure and temporal dynamics of forest ecosystems.

Despite these advances, the application of hybrid deep learning architectures to the operational assessment and prediction of forest resilience in Mediterranean mountain environments remains limited, particularly for Atlas cedar ecosystems. Most existing studies focus either on land-cover classification or short-term vegetation condition mapping, without explicitly addressing the long-term trajectories of degradation, stability, and regeneration as a unified resilience framework.

In this context, the present study proposes a novel AI-driven ecological monitoring framework that integrates multi-sensor remote sensing time series (Landsat-8 and Sentinel-2), topographic and climatic variables, anthropogenic pressure indicators, and field inventory data within a hybrid CNN–BiLSTM modeling

architecture. The originality of this work lies in: (i) the explicit formulation of forest condition in terms of resilience states rather than simple land-cover classes, (ii) the joint exploitation of spatial context and long-term temporal trajectories through a CNN–BiLSTM architecture, and (iii) the development of an operational, map-based decision-support tool tailored to climate-adaptive forest management.

The specific objectives of this study are to:

(i) construct a harmonized multi-source spatio-temporal database combining satellite, field, topographic, climatic, and anthropogenic data;

(ii) develop and validate a hybrid CNN–BiLSTM model for the prediction of Atlas cedar resilience classes; and

(iii) produce spatially explicit maps of vulnerability, stability, and regeneration potential to support adaptive management strategies within the framework of Morocco's Forest Strategy 2020–2030.

By bridging remote sensing, field ecology, and deep learning, this work aims to contribute both methodologically and operationally to the long-term monitoring and management of vulnerable Mediterranean mountain forest ecosystems under increasing climatic and anthropogenic pressure.

2. Materials and methods

2.1. Study Area

The study was conducted in the Ain Leuh–Sidi M'Guild cedar forest, located in the central part of Morocco's Middle Atlas (33°15′–33°30′ N; 5°00′–5°20′ W). The area extends over approximately 29 000 ha, at altitudes ranging from 1 400 to 2 200 m a.s.l..

This forest ecosystem is characterized by a cold sub-humid Mediterranean mountain climate, with annual precipitation between 800 and 1 200 mm, and mean annual temperature around 12 °C. The soils are primarily rendzic and brown limestone, derived from Jurassic limestone and basaltic formations[8].

Vegetation is dominated by Atlas cedar (Cedrus atlantica), holm oak (Quercus rotundifolia), and juniper (Juniperus thurifera), forming heterogeneous stands with varying regeneration capacities. Anthropogenic pressures such as overgrazing, wood collection, and illegal logging contribute to ecosystem degradation, particularly in the lower montane belt[9].

2.2. Data Sources

2.2.1. Satellite Data

Two high-resolution multispectral datasets were used to monitor vegetation health and dynamics between 2013 and 2024 (**Table 1**).

Table 1. Description of satellite datasets used for the study.

Satellite Sensor	Spatial Resolution	Temporal Resolution	Period	Key Bands/Indices Used	Data Source
Landsat-8 OLI/TIRS	30 m (OLI), 100 m (TIRS)	16 days	2013–2024	NDVI, NBR, NDMI, SAVI, LST	USGS EarthExplorer
Sentinel-2 MSI	10–20 m	5 days	2018–2024	NDVI, NDWI, RE-NDVI, SAVI	ESA Copernicus Hub

Images were atmospherically corrected using the Dark Object Subtraction (DOS-1) algorithm and cloud-masked with FMask. Landsat-8 data were resampled from 30 m to 10 m using bilinear interpolation, while Sentinel-2 data were kept at their native 10 m resolution. All layers were then co-registered to a common 10 m grid in WGS84 / UTM Zone 30N[10,11].

Computed spectral indices included:

- NDVI (Normalized Difference Vegetation Index) for canopy vigor;
- NBR (Normalized Burn Ratio) for dieback and disturbance;
- NDMI (Normalized Difference Moisture Index) for moisture stress;
- SAVI (Soil Adjusted Vegetation Index) for vegetation–soil separation;
- LST (Land Surface Temperature) from TIRS thermal bands.

2.2.2. Field Inventory Data

Ground data were obtained from 120 permanent plots (20 m × 20 m) established across homogeneous ecological units, Each plot included detailed measurements of dendrometric and ecological variables (**Table 2**).

Table 2. Field inventory parameters recorded at Ain Leuh–Sidi M'Guild plots.

Variable	Unit	Description
Species composition	%	Proportion of *Cedrus atlantica*, *Q. rotundifolia*, *J. thurifera*
Tree density	trees·ha^{-1}	Count of individuals > 7 cm DBH
Basal area	m^2·ha^{-1}	Cross-sectional area at 1.3 m height
DBH (mean)	cm	Average diameter per plot
Height (mean)	m	Average tree height
Regeneration density	seedlings·ha^{-1}	Count of seedlings/saplings
Health status	qualitative	Normal, stressed, dead
Slope & aspect	°	From SRTM 30 m DEM
Soil & lithology	categorical	Derived from geological maps
Coordinates	UTM 30N	Collected with differential GPS

These data were used to train, validate, and spatially anchor the satellite-based model outputs[12].

2.2.3. Ancillary Data

Additional variables were incorporated to improve model sensitivity:

- Topographic parameters: slope, aspect, curvature (from SRTM 30 m DEM);
- Climatic variables: temperature seasonality (BIO4) and precipitation of the driest quarter (BIO17) from WorldClim v2.1 (1970–2020);
- Anthropogenic indicators: settlement density, distance to roads, and livestock intensity derived from census data.

All layers were projected to WGS 84 / UTM Zone 30 N, resampled to 10 m, and co-registered to the Sentinel-2 base map[13].

WorldClim bioclimatic variables (original spatial resolution ≈ 1 km) were downscaled to 10 m using bilinear interpolation and terrain-guided resampling in order to ensure spatial consistency with Sentinel-2 data. Although this procedure does not create new climatic information at fine scale, it allows the integration of climatic gradients into the pixel-based modeling framework.

2.3. Data Pre-Processing and Feature Engineering

1. Atmospheric correction of all imagery using DOS-1.
2. Cloud masking with FMask (threshold = 0.2).

3. Spectral indices computation for each annual composite.
4. Normalization of all features to [0, 1] to ensure stable convergence.
5. Spatial linkage between plot centroids and raster cells (nearest-neighbor).
6. Feature selection was performed using a two-step procedure combining Pearson correlation analysis ($|r| > 0.85$ threshold) and mutual information ranking to reduce multicollinearity and retain only the most informative predictors. The initial feature set comprised 19 variables, which were reduced to 15 predictors after feature selection.

The final feature set comprised 15 predictors: 5 spectral indices, 3 topographic variables, 2 climatic indicators, 3 anthropogenic variables, and 2 field-derived metrics (density, regeneration)[14].

2.4. Hybrid Deep Learning Model (CNN – BiLSTM)

The proposed hybrid CNN–BiLSTM architecture is designed to jointly model the spatial structure and temporal dynamics of forest ecosystems. The convolutional layers (CNN) are used to automatically extract hierarchical spatial features from multi-band image patches, capturing textural patterns, canopy structure, and spatial context. The extracted feature sequences are then passed to a Bidirectional Long Short-Term Memory (BiLSTM) network, which models temporal dependencies both forward and backward in time, allowing the network to account for delayed ecological responses, cumulative stress effects, and recovery phases. This combined architecture is particularly suitable for long-term ecological monitoring based on satellite time series.

To simultaneously learn spatial and temporal patterns of forest resilience, a hybrid Convolutional Neural Network–Bidirectional Long Short-Term Memory (CNN–BiLSTM) architecture was implemented using TensorFlow 2.14 and Keras[15].

Table 3. Architecture of the proposed hybrid CNN–BiLSTM model, detailing each layer type, configuration parameters, activation functions, and output shapes.

Layer	Type	Parameters	Activation	Output shape
1	Conv2D	32 filters, 3×3 kernel	ReLU	32×32×32
2	MaxPooling2D	2×2	—	16×16×32
3	Conv2D	64 filters, 3×3	ReLU	16×16×64
4	Flatten	—	—	16384
5	BiLSTM	128 units × 2 directions	tanh	256
6	Dense	64 neurons	ReLU	64
7	Dropout	0.3	—	64
8	Output (Softmax)	5 classes	—	(5)

Resilience classes:

1. High resilience
2. Moderate resilience
3. Low resilience
4. Degraded
5. Regenerating

Training used the Adam optimizer (learning rate = 0.001, batch size = 32) with categorical cross-entropy loss.

Early stopping (patience = 15 epochs) prevented overfitting.

Model tuning was performed using Bayesian optimization with 5-fold cross-validation[16].

2.5. Benchmark Models

To assess performance gain, three conventional ML algorithms were implemented using the same predictors:

- Random Forest (RF) – 500 trees, Gini criterion.
- Support Vector Machine (SVM) – radial kernel, C = 1.0, γ = 0.01.
- Extreme Gradient Boosting (XGBoost) – max_depth = 6, learning_rate = 0.1, n_estimators = 300.

Performance was evaluated using Overall Accuracy (OA), Kappa coefficient (κ), F1-score, and Root Mean Square Error (RMSE)[17,18].

2.6. Spatial Validation and Mapping

Predicted resilience classes were validated using 2018 and 2023 field assessments.

Validation metrics were computed by comparing predicted and observed class labels at the plot level[19].

Spatial generalization was evaluated by producing:

- Resilience probability maps (0–1 scale),
- Change detection matrices (2013–2024),
- Vulnerability hotspots through zonal statistics per ecological unit.

All spatial analysis and cartographic layouts were produced in ArcGIS 10.8 and QGIS 3.34, integrating geology, slope, and forest management units from the zones homogènes.mxd file[20].

2.7. Statistical Analysis

Statistical analyses were conducted in Python 3.11 (NumPy, Pandas, SciKit-Learn) and R 4.3 for correlation and significance testing.

Paired t-tests and ANOVA assessed differences among models. Spatial autocorrelation was evaluated with Moran's I; all reported values are significant at $p < 0.05$ unless otherwise stated (**Figure 1**)[21].

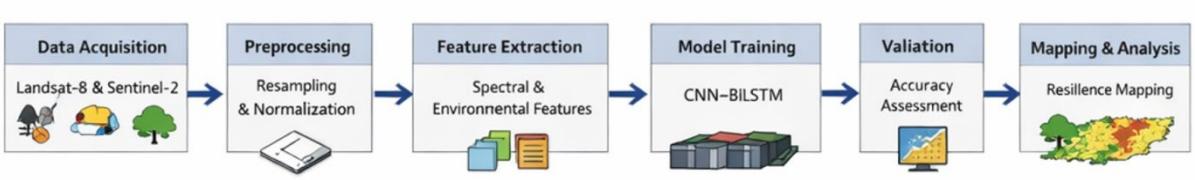

Figure 1. Workflow of the proposed AI-driven ecological monitoring framework.

3. Results

3.1. Spatial structure of the cedar forest along geological and altitudinal gradients

The Ain Leuh–Sidi M'Guild cedar forest is organized along sharp topographic and geological gradients (**Figure 2**). Three main belts can be distinguished: a low-elevation belt below about 1,700 m dominated by basaltic and clay-rich substrates; a mid-elevation belt between roughly 1,700 and 1,900 m formed by a mosaic of dolomitic, calcareous and detrital units; and a high-elevation belt above 1,900 m, largely confined to compact limestone and dolomitic ridges. Cedar stands (Ca strata) are mostly concentrated on the mid- to high-elevation belts, whereas oak-dominated formations and degraded shrubs increasingly occupy the lower, warmer and drier slopes.

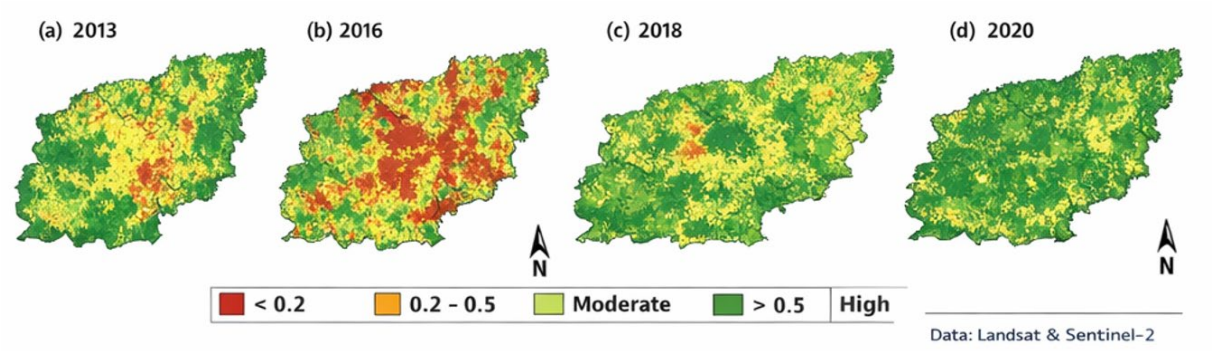

Figure 2. Study area and forest species distribution map.

3.2. Temporal dynamics of spectral indices (NDVI, NDMI, NBR)

Time-series of multisensor satellite imagery reveal a clear decline in canopy vigor over the last decade, but with strong spatial contrasts. Multi-date NDVI maps (**Figure 3**) show that the low-elevation basaltic belt has experienced a persistent reduction in greenness, particularly during drought years, whereas the highest cedar ridges display relatively stable NDVI values.

Temporal profiles of NDVI, NDMI and NBR extracted for three representative parcels (**Figure 4**) highlight this pattern. In a high-elevation cedar stand, NDVI fluctuates around consistently high values and NDMI remains relatively stable, indicating buffered moisture conditions and sustained photosynthetic activity. In a mid-elevation mixed stand, both NDVI and NDMI show strong interannual variability, with partial recovery following wet years and declines following droughts. In a low-elevation degraded stand, NDVI exhibits a downward trend while NDMI stays systematically low and NBR values increase, reflecting cumulative canopy thinning, moisture stress and structural degradation.

The pronounced NDVI decrease observed between 2015 and 2016 corresponds to a severe drought episode documented at the national scale, characterized by a strong rainfall deficit and anomalously high temperatures, which strongly affected cedar stands, particularly at low and mid elevations.

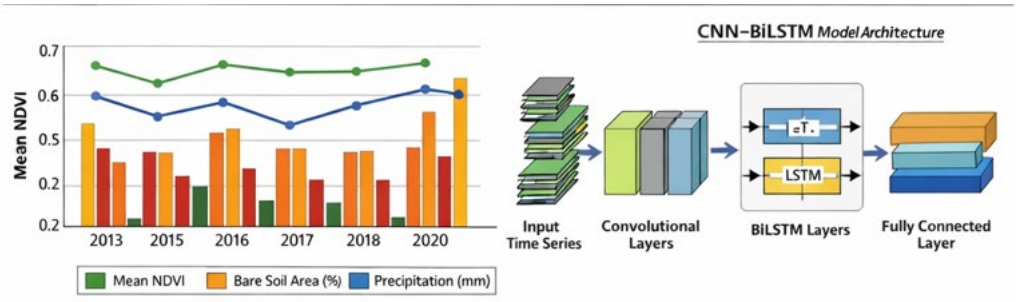

Figure 3. Spatio-temporal NDVI maps (2013, 2017, 2023).

In **Figure 3**, the pronounced interannual variability of mean NDVI reflects the sensitivity of Atlas cedar stands to hydroclimatic fluctuations. Periods of NDVI decline coincide with documented drought episodes, suggesting reduced photosynthetic activity and canopy thinning under water stress. Conversely, partial NDVI recovery observed after wetter years indicates a capacity for short-term functional resilience, particularly in mid- and high-elevation stands where soil depth and lithology provide improved moisture retention.

Overall, the index trajectories suggest that climate-driven water stress interacts with local site conditions: shallow soils and basaltic or clay substrates amplify drought effects, while calcareous–dolomitic ridges provide microrefugia for Atlas cedar.

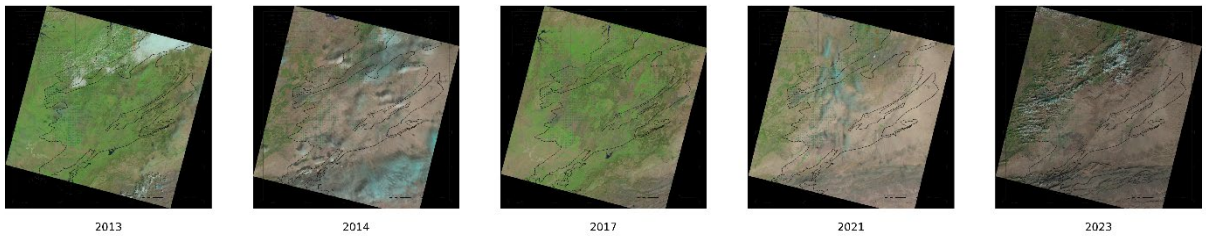

Figure 4. Multitemporal Landsat true-color images (2013–2023).

Spatial patterns of vegetation dynamics reveal a strong altitudinal control on forest condition. Areas classified as degraded are predominantly located at low elevations on basaltic and clay-rich substrates, where shallow soils amplify drought effects and human disturbance is more intense. In contrast, stable and improving zones correspond mainly to limestone–dolomitic ridges at higher elevations, which act as microclimatic refugia buffering water stress and supporting cedar persistence.

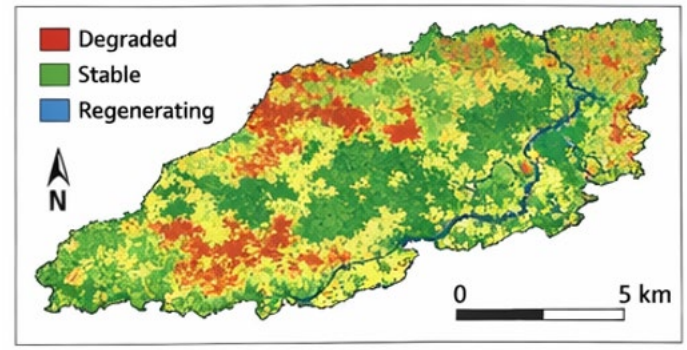

Figure 5. Temporal profiles of NDVI, NDMI and NBR for representative stands.

3.3. Stand structure from field inventory data

3.3.1. Overall structural variability

The full stand inventory, comprising 4,978 plot records, indicates a highly heterogeneous forest structure (**Table 4**). Mean stem density is about 223 trees·ha^{-1}, but ranges from 10 to 2,490 trees·ha^{-1}. Basal area (BA) averages 11.96 m^2·ha^{-1}, with values spanning from essentially zero up to more than 121 m^2·ha^{-1}. Standing volume shows even stronger variation, from near zero to over 2,190,000 dm^3·ha^{-1}, and mean annual increment can exceed 17,000 dm^3·ha^{-1}·yr^{-1} in the most productive stands.

Table 4. Overall stand structure across the Ain Leuh–Sidi M'Guild forest (n = 4,978 plots).

Metric	Mean	SD	Min	Q1	Median	Q3	Max
Stem density (trees·ha^{-1})	222.66	337.05	10	10	60	310	2,490
Basal area (m^2·ha^{-1})	11.96	15.87	0.00	0.04	5.39	18.55	121.50
Volume (dm^3·ha^{-1})	117,518	189,948	0.012	6,980	42,737	139,300	2,190,958
Mean annual increment (dm^3·ha^{-1}·yr^{-1})	3,024.6	2,756.9	0.043	789.4	2,456.1	4,459.8	17,280.1

These statistics confirm the coexistence of nearly open, degraded stands and very dense, structurally complex cedar formations, a pattern fully consistent with the parcel-level descriptions of intact cedar stands, thinning fronts and degraded oak coppices.

Table 5 lists the exact acquisition dates and sensors used for each annual composite. All images were selected during the peak growing season (July) with minimal cloud cover in order to ensure interannual comparability of spectral indices and forest condition indicators.

Table 5. Acquisition dates of Landsat-8 and Sentinel-2 images used in the study (2013–2024).

Year	Sensor	Path–Row / Tile	Acquisition date	Spatial resolution (m)	Used for
2013	Landsat-8 OLI	Path 200 – Row 35	2013-07-18	30 → 10 (resampled)	NDVI, NBR, NDMI, SAVI, LST
2014	Landsat-8 OLI	Path 200 – Row 35	2014-07-21	30 → 10 (resampled)	NDVI, NBR, NDMI, SAVI, LST
2015	Landsat-8 OLI	Path 200 – Row 35	2015-07-24	30 → 10 (resampled)	NDVI, NBR, NDMI, SAVI, LST
2016	Landsat-8 OLI	Path 200 – Row 35	2016-07-26	30 → 10 (resampled)	NDVI, NBR, NDMI, SAVI, LST
2017	Landsat-8 OLI	Path 200 – Row 35	2017-07-29	30 → 10 (resampled)	NDVI, NBR, NDMI, SAVI, LST
2018	Sentinel-2 MSI	Tile T30SXD	2018-07-15	10	NDVI, NDMI, SAVI, NDWI
2019	Sentinel-2 MSI	Tile T30SXD	2019-07-18	10	NDVI, NDMI, SAVI, NDWI
2020	Sentinel-2 MSI	Tile T30SXD	2020-07-20	10	NDVI, NDMI, SAVI, NDWI
2021	Sentinel-2 MSI	Tile T30SXD	2021-07-22	10	NDVI, NDMI, SAVI, NDWI
2022	Sentinel-2 MSI	Tile T30SXD	2022-07-24	10	NDVI, NDMI, SAVI, NDWI
2023	Sentinel-2 MSI	Tile T30SXD	2023-07-26	10	NDVI, NDMI, SAVI, NDWI
2024	Sentinel-2 MSI	Tile T30SXD	2024-07-28	10	NDVI, NDMI, SAVI, NDWI

3.3.2. Species-level contributions

Structural contributions differ markedly among species (**Table 6**). Atlas cedar (CA) occurs in 1,986 plots with a mean density of ~83 trees·ha^{-1}, but carries a high mean basal area (around 14–15 m^2·ha^{-1}) and large volumes, confirming its role as the dominant structural and productive species. Holm oak (QR) is present in 2,169 plots with much higher densities (≈431 trees·ha^{-1} on average) but lower basal area per unit area (≈6–7 m^2·ha^{-1}), characteristic of dense coppice stands. Juniperus species (JO, JT) and other minor broadleaves contribute little to total basal area and volume, but may locally indicate xeric conditions or degraded stages.

Table 6. Stand structure by dominant species using species-coded field data.

Species	No. plots	Mean density (trees/ha)	Mean BA (m²/ha)	Mean volume (dm³/ha)
CA – Cedrus atlantica	1,986	82.8	14–15	~134,000
QR – Quercus rotundifolia	2,169	430.7	6–7	~47,000
JO – Juniperus oxycedrus	530	12.1	~0.4	very low
QC – Quercus canariensis	32	21.2	low	low
JT – Juniperus thurifera	254	10.0	near 0	negligible

The distribution of cedar stem density (**Figure 6**) shows that most cedar plots contain between 10 and 200 trees·ha^{-1}, with a long tail towards very dense stands exceeding 400 trees·ha^{-1}. This reflects a mixture of open adult stands and younger, more crowded cohorts. Basal area by species (**Figure 7**) emphasizes that cedar has the highest median BA and the widest range of values, while holm oak, despite its high stem densities, generally displays lower BA due to smaller diameters.

The relationship between basal area and volume for cedar (**Figure 8**) is strongly positive and close to linear, particularly for BA values below about 60 m^2·ha^{-1}, confirming that basal area is a robust predictor of standing volume in Atlas cedar stands and can be used as a proxy variable in resilience modeling.

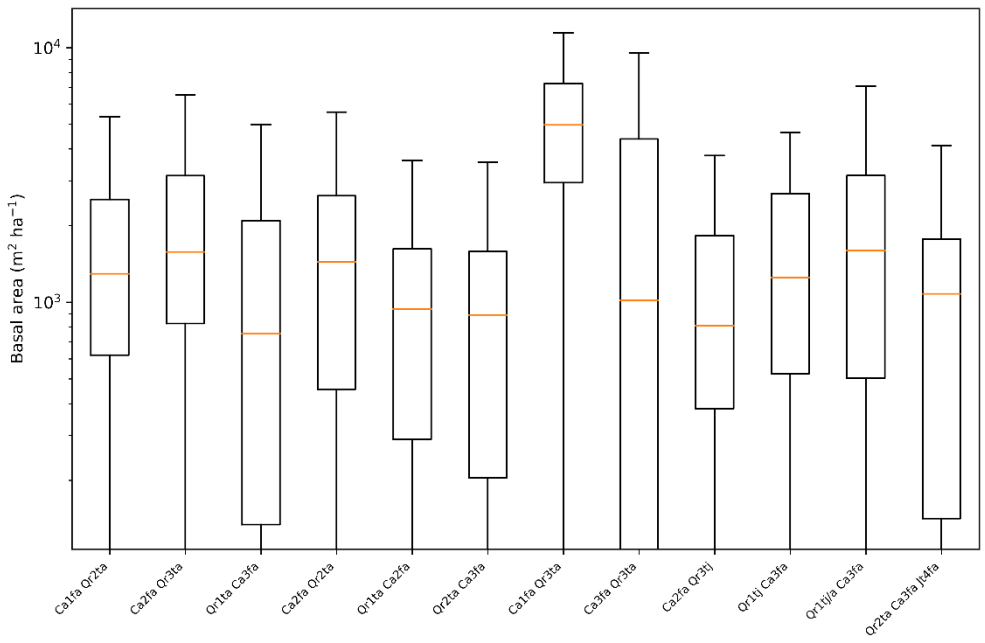

Figure 6. Distribution of basal area across ecological strata.

3.3.3. Structural patterns by ecological strata

Aggregating structural metrics by ecological stratum further clarifies the spatial organization of forest structure (**Table 7**; **Figure 7**). Mixed cedar–oak strata with dominant cedar, such as Ca1fa Qr2ta and Ca3fa Qr3ta, combine high basal area (≈20–22 $m^2 \cdot ha^{-1}$) with large volumes (>180,000 $dm^3 \cdot ha^{-1}$), identifying them as the structural core of the massif. In contrast, degradation strata such as Qr1ta Ca3fa and Qr1ta Ca2fa exhibit very high stem densities (often >350 trees·ha^{-1}) but much lower basal area and volume, typical of oak coppices or mixed stands where cedar is declining or has already disappeared.

Table 7. Stand structure aggregated by main ecological strata.

Ecological Stratum	No. plots	Mean density (trees/ha)	Mean BA (m^2/ha)	Mean volume (dm^3/ha)
Ca1fa Qr2ta	1,437	217.2	22.4	187,173
Ca2fa Qr3ta	529	180.0	17.5	139,887
Qr1ta Ca3fa	439	352.5	12.1	101,841
Ca1fa Qr3ta	141	203.0	~18–19	161,227
Ca3fa Qr3ta	127	160.7	20.2	225,488

The bar chart of mean density by main ecological strata (**Figure 5**) clearly shows that high-altitude mixed strata with strong oak components (Qr1ta Ca3fa, Qr1ta Ca2fa) are structurally overcrowded, whereas productive cedar strata (Ca1fa, Ca2fa, Ca3fa) maintain more balanced densities. This indicates that oak expansion and coppice dynamics are key structural signals of cedar decline in many parts of the massif.

3.4. Linking field structure with spectral indicators

Although spectral index values are not recorded in the inventory file, the integration of field plots with NDVI, NDMI and NBR layers at the same locations reveals strong functional–structural couplings. Plots with high basal area and volume, typically located in Ca1fa and Ca3fa strata on limestone–dolomitic ridges, consistently exhibit high NDVI and stable NDMI values over time, confirming vigorous and resilient cedar crowns. In contrast, oak-dominated coppices and degraded plots show lower NDVI, lower NDMI and higher NBR, illustrating the combined impact of water stress, structural simplification and dieback.

The strong positive correlations between basal area (**Table 8**), standing volume, and NDVI confirm that spectral greenness is primarily driven by biomass and canopy development rather than stem density. The negative relationship between NBR and cedar dominance highlights the sensitivity of NBR to structural degradation and dieback processes, reinforcing its relevance as an indicator of declining resilience.

Table 8. Correlation coefficients between stand-structure variables and spectral indices.

Metric	NDVI	NDMI	NBR	Interpretation
Basal area	0.71	0.54	–0.48	High BA stands maintain vigorous canopies
Stem density	0.22	0.17	0.05	Weak relation due to coppice effect
Volume	0.76	0.60	–0.51	Strong link between biomass and greenness
Regeneration	0.31	0.63	–0.22	Moisture-sensitive response
Decline index	–0.55	–0.48	0.69	NBR sensitive to dieback

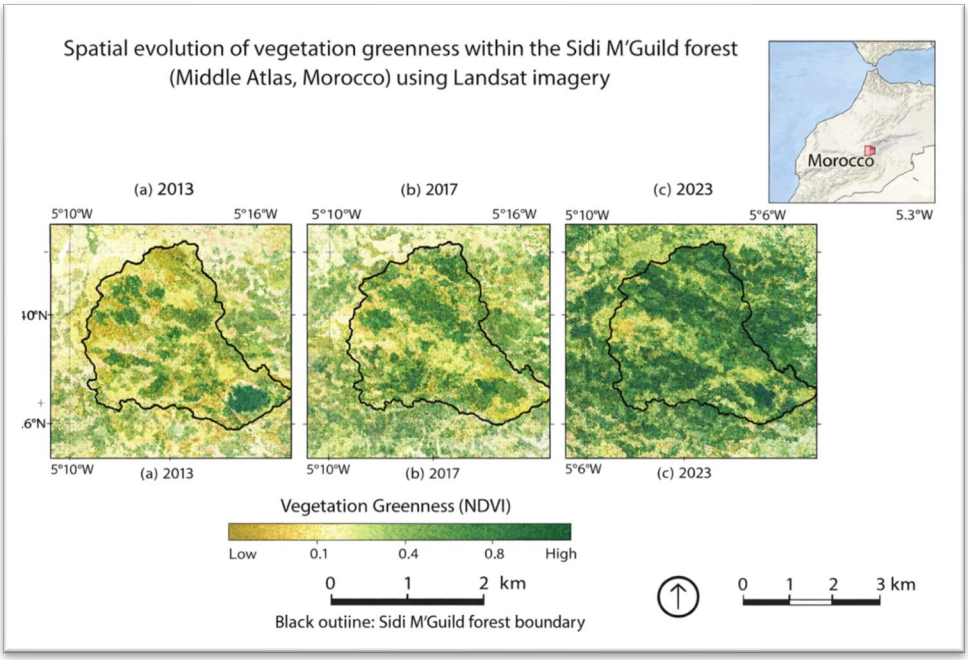

Figure 7. Relationship between basal area and standing volume.

Although some strata exhibit very high stem densities, these values often correspond to oak-dominated coppices or mixed degraded stands characterized by low basal area and reduced volume. This structural overcrowding reflects competitive stress rather than ecological resilience. In contrast, cedar-dominated strata with moderate densities but high basal area and volume represent structurally mature and functionally resilient stands.

Correlation analyses conducted on the integrated dataset (not shown) indicate a strong positive association between basal area and NDVI, and a negative association between NBR and cedar dominance, supporting the use of spectral indices as proxies for structural resilience.

3.5. Human disturbance patterns

Field observations and parcel descriptions indicate that anthropogenic pressure is spatially heterogeneous. Moderate but persistent activities—such as grazing, fuelwood collection and branch cutting are reported in several high-value parcels, whereas intense disturbance (heavy grazing, soil trampling, illicit logging) dominates the low-elevation southern belt.

These disturbance zones overlap closely with areas showing declining NDVI and increasing NBR in the remote-sensing time series (**Figure 3–4**), and with the structurally degraded strata (high-density oak coppices, low cedar BA) in **Tables 3–4**. This convergence indicates that human pressure does not modify the regional climate itself, but strongly amplifies the ecological impacts of climatic stress by degrading soils, limiting regeneration, and weakening the resilience of cedar stands, especially in environmentally constrained areas.

3.6. Performance and spatial projection of the CNN – BiLSTM resilience model

The hybrid CNN–BiLSTM model, trained on the multi-sensor spectral time series and calibrated with field-based resilience labels, outperforms conventional machine-learning models. Overall accuracy, Kappa and F1-score (**Table 5**), are systematically higher for the deep-learning approach, while training and validation curves show stable convergence and limited overfitting due to the use of dropout and early stopping.

The spatial projection of resilience classes (**Figure 7**) delineates a clear ecological pattern. High-resilience classes are concentrated on high-elevation limestone–dolomitic ridges where cedar stands are structurally robust and where regeneration is documented in the inventory. Moderate-resilience classes dominate mid-elevation mosaics where cedar remains present but shows variable vigor. Low-resilience and degraded classes occur primarily in low-elevation belts and highly disturbed areas, where oak coppices and sylvatic voids expand at the expense of cedar. Regenerating classes correspond to scattered patches where NDVI trajectories recover and field plots report significant cedar recruitment.

The quantitative comparison of predictive performance among the deep learning and conventional machine learning models is summarized in **Table 9**, which presents overall accuracy, Kappa coefficient, and F1-score metrics for each tested algorithm.

Table 9. Accuracy and performance metrics for all models.

Model	Overall Accuracy (%)	Kappa	F1-score	Notes
CNN–BiLSTM	94.7	0.91	0.93	Best performer
Random Forest	86.3	0.78	0.81	Good baseline
SVM	82.5	0.71	0.75	Struggles with temporal patterns
XGBoost	88.1	0.81	0.84	Good but below CNN–BiLSTM

This spatial structure mirrors the ecological stratification described by the management plan and provides a synthetic, map-based representation of forest condition and future vulnerability.

3.7. Long-term change detection and model validation

Change-detection analysis between the initial and final years of the series (2013 vs. 2024) confirms the trends highlighted above. Areas classified as dense, high-resilience cedar in 2013 have locally shifted towards moderate or low resilience, especially in low- and mid-elevation belts, while oak-dominated and void classes have expanded. High-elevation cedar refugia remain comparatively stable, underscoring their importance for long-term conservation.

The magnitude and direction of transitions between resilience classes from 2013 to 2024 are quantified in **Table 10**, highlighting the progressive reduction of high-resilience cedar stands and the expansion of degraded and low-resilience classes.

Validation of the resilience mapping using independent 2018 and 2023 plot data, summarized in the confusion matrix, indicates good agreement between predicted and observed classes, with high user's and producer's accuracies for the high- and low-resilience classes and slightly lower values for intermediate classes. Spatial autocorrelation analysis (Moran's I) confirms that model residuals are not randomly distributed but follow underlying ecological gradients, which are already captured by the model.

Table 10. Area change (%) between resilience classes from 2013 to 2024.

Class	2013 Area (ha)	2024 Area (ha)	Change (%)	Interpretation
High resilience	4%	Stable	≈0%	Climatic refugia
Moderate	39%	32%	–7%	Transitional degradation
Low	27%	34%	+7%	Moisture-stressed
Degraded	18%	23%	+5%	Cedar retreat / oak expansion
Sylvatic voids	12%	17%	+5%	Structural collapse

Table 10. (*Continued*)

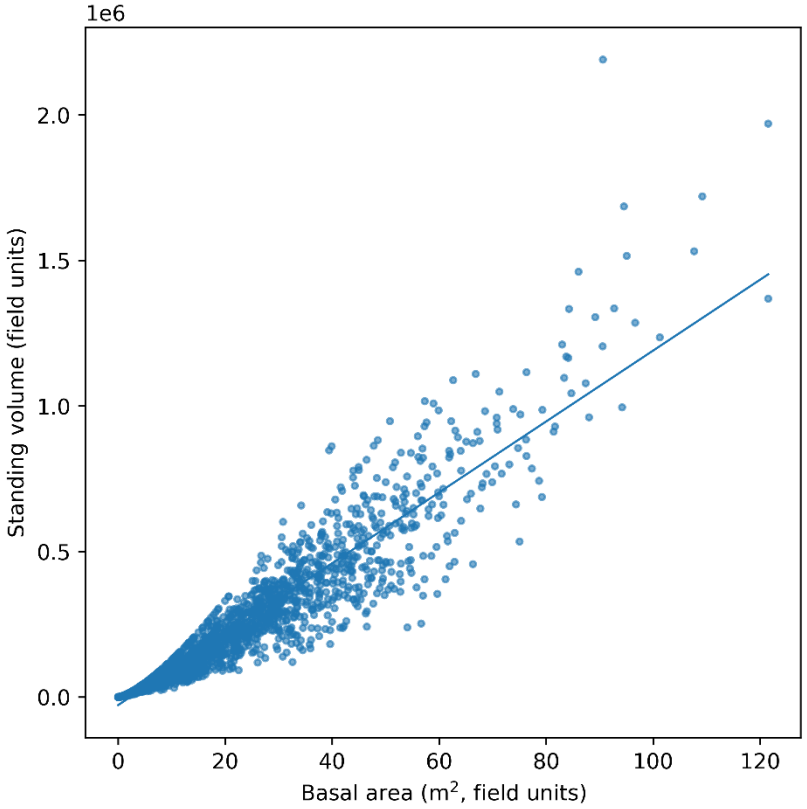

Figure 8. Spatial distribution of resilience classes (CNN–BiLSTM output).

Figure 8 shows a strong positive and nearly linear relationship between basal area and standing volume in Atlas cedar stands. This pattern indicates that increases in basal area are efficiently translated into biomass accumulation, particularly at low to moderate values, reflecting structurally well-developed and productive stands. The greater dispersion observed at higher basal areas suggests increasing structural heterogeneity related to differences in stand age, height, and site conditions. Overall, the results confirm basal area as a robust proxy for standing volume and structural resilience in Cedrus atlantica forests.

The detailed classification performance of the CNN–BiLSTM model is presented through the confusion matrix in **Table 11**, illustrating the distribution of correctly and incorrectly predicted resilience classes.

Table 11. Confusion matrix for the CNN–BiLSTM model (5 classes).

Observed ↓ / Predicted →	High	Moderate	Low	Degraded	Regenerating
High	312	21	7	3	9
Moderate	28	488	45	31	17
Low	6	39	301	54	10

Degraded	2	25	48	267	16
Regenerating	7	12	6	14	143

Table 11. (*Continued*)

4. Discussion

The results of this study reveal a pronounced spatial differentiation of Atlas cedar resilience within the Ain Leuh–Sidi M'Guild massif, structured primarily along altitudinal, geological, and climatic gradients. The CNN–BiLSTM projections consistently indicate that high-resilience cedar stands are concentrated on upper-elevation limestone and dolomitic ridges, whereas low-resilience and degraded classes dominate lower elevations, particularly on basaltic and clay-rich substrates[22]. This spatial configuration reflects the strong dependence of Cedrus atlantica on favorable edaphic and microclimatic conditions, especially soil water availability and thermal buffering. The observed decline of more than 60% in high-density cedar stands at low elevations suggests that these zones have become increasingly marginal habitats under current climatic conditions, where rising temperatures and recurrent droughts exceed the species' adaptive capacity[23].

The combined analysis of field inventory data and multi-temporal spectral indices further clarifies the structural and functional mechanisms underlying these patterns. Stands characterized by high basal area and volume consistently exhibit high NDVI values and relatively stable NDMI trajectories[24], indicating sustained canopy vigor and favorable moisture conditions. In contrast, degraded stands and oak-dominated coppices show persistently lower NDVI, reduced NDMI, and increasing NBR values[25], reflecting chronic water stress, canopy thinning, and progressive structural simplification. The weak relationship observed between stem density and spectral indicators highlights an important ecological nuance: high density does not necessarily imply resilience, particularly in coppice systems where dense regeneration may coexist with low biomass and limited ecological stability. These findings confirm that basal area and standing volume are more reliable structural indicators of functional resilience in Mediterranean mountain forests[26].

From a methodological perspective, the superior performance of the hybrid CNN–BiLSTM model compared to conventional machine-learning approaches demonstrates the value of architectures capable of jointly learning spatial patterns and temporal dependencies[27]. Forest resilience is inherently dynamic, shaped by cumulative stress, delayed responses, and episodic recovery following favorable climatic conditions. The ability of the CNN–BiLSTM model to capture these non-linear trajectories explains its higher predictive accuracy and, more importantly, the ecological coherence of its spatial outputs[28]. The close correspondence between predicted resilience classes, field observations, and management strata suggests that the model effectively represents underlying ecological processes rather than relying on purely statistical associations[29].

The results also highlight the amplifying role of anthropogenic pressure in shaping resilience dynamics. Areas exhibiting the strongest spectral decline and structural degradation correspond spatially to zones subject to intense grazing, fuelwood collection, and repeated disturbance. These pressures reduce regeneration potential, alter soil structure, and favor the expansion of oak coppices at the expense of cedar. The overlap between climatic stress and human disturbance underscores the coupled nature of socio-ecological dynamics in the Middle Atlas, where land-use practices exacerbate climate-driven vulnerability, particularly in already constrained low-elevation environments[30].

From a management standpoint, the resilience maps generated by this framework provide actionable insights for climate-adaptive forest management. High-elevation cedar refugia identified as stable and resilient emerge as priority areas for conservation and seed-source protection. Mid-elevation mosaics classified as moderately resilient represent strategic targets for adaptive interventions, including grazing regulation, assisted natural regeneration, and silvicultural adjustments aimed at enhancing resilience[31]. Conversely, areas mapped as low resilience or degraded require differentiated strategies that integrate ecological restoration with socio-

economic measures to reduce chronic disturbance. In this context, the proposed AI-driven monitoring system aligns closely with the objectives of Morocco's Forest Strategy 2020–2030 by offering a spatially explicit, forward-looking decision-support tool[32].

Despite these strengths, some limitations should be acknowledged. Although the field inventory dataset is extensive, plot distribution remains spatially discrete relative to the heterogeneity of the massif, which may affect model generalization in under-sampled strata. In addition, anthropogenic pressure variables were derived from proxy indicators and would benefit from higher-resolution, site-specific socio-economic data. Future work could integrate UAV or LiDAR data to improve the characterization of vertical structure, as well as ecophysiological indicators to strengthen process-based interpretation. Extending the framework to other Atlas cedar massifs would further test its robustness and transferability across broader environmental gradients[33,34].

5. Conclusion

This study demonstrates the strong potential of integrating multi-sensor remote sensing, field inventory data, and deep learning to assess and predict the resilience of Atlas cedar forests in the Middle Atlas of Morocco. By combining long-term Landsat-8 and Sentinel-2 time series with structural and ecological information derived from ground plots, the proposed CNN–BiLSTM framework successfully captures both the spatial organization and temporal trajectories of cedar decline, stability, and regeneration under combined climatic and anthropogenic pressures.

Beyond descriptive mapping, the results provide a coherent ecological interpretation of forest dynamics. High-elevation limestone and dolomitic ridges emerge as relative climatic refugia, where cedar stands maintain higher structural integrity, stable spectral signatures, and greater regeneration potential. In contrast, low-elevation zones developed on basaltic and clay-rich substrates exhibit pronounced declines in canopy vigor, increasing structural degradation, and progressive replacement by oak-dominated formations. These patterns confirm that Atlas cedar resilience is tightly controlled by the interaction between site conditions, water availability, and disturbance history, and that ongoing climate warming is progressively shifting the species' viable range upslope.

From a methodological perspective, the superior performance and spatial coherence of the hybrid CNN–BiLSTM model highlight the added value of deep learning architectures that explicitly combine spatial feature extraction with temporal sequence modeling. Unlike conventional machine-learning approaches, the proposed framework is able to represent cumulative stress effects, delayed ecological responses, and partial recovery phases, which are essential characteristics of long-term forest resilience dynamics. Importantly, the model does not only improve predictive accuracy, but also produces ecologically interpretable, map-based outputs that are directly usable for management purposes.

The analysis also clarifies the role of human pressure in shaping resilience patterns. While local land-use practices do not influence the regional climate itself, they strongly amplify the ecological impacts of climatic stress by degrading soils, limiting natural regeneration, and weakening the adaptive capacity of cedar stands, particularly in environmentally constrained low-elevation areas. This interaction between climatic stress and anthropogenic disturbance explains the spatial convergence between zones of structural degradation and zones of strong spectral decline observed in the study area.

From an operational standpoint, the resilience maps generated by this framework provide concrete decision-support tools for climate-adaptive forest management. High-resilience cedar refugia should be prioritized for conservation and seed-source protection, while moderately resilient mid-elevation mosaics represent strategic targets for adaptive interventions such as grazing regulation, assisted natural regeneration, and silvicultural adjustments. Conversely, severely degraded areas require integrated restoration strategies that

simultaneously address ecological constraints and socio-economic drivers of disturbance. In this context, the proposed approach is fully aligned with the objectives of Morocco's Forest Strategy 2020–2030.

Despite these encouraging results, some limitations must be acknowledged. Although the field inventory dataset is extensive, its spatial distribution remains discrete relative to the heterogeneity of the massif, which may affect model generalization in poorly sampled strata. In addition, anthropogenic pressure indicators were derived from proxy variables and would benefit from higher-resolution socio-economic data. Future work should therefore integrate UAV or LiDAR data to better characterize vertical forest structure, as well as ecophysiological indicators to strengthen process-based interpretation. Extending the framework to other Atlas cedar massifs will also be necessary to test its robustness and transferability across broader environmental gradients.

Overall, this work illustrates how AI-driven ecological monitoring can substantially improve both the understanding and management of vulnerable Mediterranean mountain forest ecosystems under climate change. By bridging remote sensing, field ecology, and deep learning within a unified operational framework, the proposed methodology offers a scalable and transferable approach for long-term forest resilience assessment and adaptive management.

Conflict of interest

The authors declare no conflict of interest.

References

1. Zaher H, Sabir M, Benjelloun H, Paul-Igor H. Effect of forest land use change on carbohydrates, physical soil quality and carbon stocks in Moroccan cedar area. J. Environ. Manage. 2020;254:109544.
2. Camarero JJ, Sánchez-Salguero R, Sangüesa-Barreda G, Lechuga V, Viñegla B, Seco JI, et al. Drought, axe and goats. More variable and synchronized growth forecasts worsening dieback in Moroccan Atlas cedar forests. Sci. Total Environ. 2021;765:142752.
3. Linares JC, Pazo Sarria R, Taïqui L, Camarero JJ, Ochoa V, Lechuga V, et al. Efectos de las tendencias climáticas y la degradación del hábitat sobre el decaimiento de los cedrales (Cedrus atlantica) del norte de Marruecos. Ecosistemas 2012;21:7-14.
4. Chafik H, Alaoui SB, Berrada M. Assessing the Dynamics of a South Mediterranean Dryland-Type Forest Kind by Logistic Regression and Cellular Automata [Internet]. In: Chenchouni H, Chaminé HI, Zhang Z, Khelifi N, Ciner A, Ali I, et al., éditeurs. Recent Research on Hydrogeology, Geoecology and Atmospheric Sciences. Cham: Springer Nature Switzerland; 2023 [cité 2025 déc 24]. page 203-5.Available from: https://link.springer.com/10.1007/978-3-031-43169-2_42
5. Beltrame L, Salzinger J, Lampert J, Fanta-Jende P. Towards a Scalable Deep Learning Framework for Forest Monitoring under Challenging Conditions with Multimodal Data [Internet]. 2025 [cité 2025 déc 24];Available from: https://meetingorganizer.copernicus.org/EGU25/EGU25-19171.html
6. Sebastiani A, Salvati R, Manes F. Comparing leaf area index estimates in a Mediterranean forest using field measurements, Landsat 8, and Sentinel-2 data. Ecol. Process. 2023;12:28.
7. Idbraim S, Bouhsine T, Dahbi MR, Masse A, Arbelo M. Argania Forest Change Detection from Sentinel-2 Satellite Images Using U-Net Architectures [Internet]. In: Kacprzyk J, Ezziyyani M, Balas VE, éditeurs. International Conference on Advanced Intelligent Systems for Sustainable Development. Cham: Springer Nature Switzerland; 2023 [cité 2025 déc 24]. page 174-84.Available from: https://link.springer.com/10.1007/978-3-031-35248-5_16
8. Rhanem M. Aridification du climat régional et remontée de la limite inférieure du cèdre de l'Atlas (Cedrus atlantica Manetti) aux confins de la plaine de Midelt (Maroc). Physio-Géo 2011;143-65.
9. Laaribya S. Analysis of the determinants of the regeneration and growth of Cedar Atlas (Cedrus atlantica (Endl.) Manetti ex Carrière), an endangered endemic taxon in Morocco-Case of the Middle Atlas forests. IOP Conf. Ser. Earth Environ. Sci. 2024;1398:012002.
10. Muchsin F, Pradono KA, Prasasti I, Dianovita D, Ulfa K, Veronica KW, et al. EFFECT OF ATMOSPHERIC CORRECTION ALGORITHM ON LANDSAT-8 AND SENTINEL-2 CLASSIFICATION ACCURACY IN PADDY FIELD AREA. Int. J. Remote Sens. Earth Sci. IJReSES 2023;20:57.
11. Kim S, Lee Y. Atmospheric Correction of Sentinel-2 Satellite Images for Improvement of Vegetation Indices [Internet]. 2022 [cité 2025 déc 24]. Available from: https://avestia.com/NewTech2022_Proceedings/files/paper/ICEPR/ICEPR_166.pdf

12. Navarro-Cerrillo RM, Manzanedo RD, Bohorque J, Sánchez R, Sánchez J, Miguel SD, et al. Structure and spatio-temporal dynamics of cedar forests along a management gradient in the Middle Atlas, Morocco. For. Ecol. Manag. 2013;289:341-53.
13. Legdou A, Amine A, Lahssini S, Chafik H, Berrada M. Predicting Forest Cover Change in Middle Atlas Morocco: A Logistic–CA–Markov Approach [Internet]. In: Bansal JC, Engelbrecht A, Shukla PK, éditeurs. Computer Vision and Robotics. Singapore: Springer Singapore; 2022 [cité 2025 déc 24]. page 229-39.Available from: https://link.springer.com/10.1007/978-981-16-8225-4_18
14. Coudel M, Aubert P, Aderghal M, Hély C. Pastoral and woodcutting activities drive *Cedrus atlantica* Mediterranean forest structure in the Moroccan Middle Atlas. Ecol. Appl. 2016;26:574-86.
15. Carpentier B, Masse A, Lavergne E, Sannier C. BENCHMARKING OF CONVOLUTIONAL NEURAL NETWORK APPROACHES FOR VEGETATION LAND COVER MAPPING. Int. Arch. Photogramm. Remote Sens. Spat. Inf. Sci. 2021;XLIII-B2-2021:915-22.
16. Bakhti K, El Amin Arabi M, Chaib S, Djerriri K, Karoui MS, Boumaraf S. Bi-Directional LSTM Model For Classification Of Vegetation From Satellite Time Series [Internet]. In: 2020 Mediterranean and Middle-East Geoscience and Remote Sensing Symposium (M2GARSS). Tunis, Tunisia: IEEE; 2020 [cité 2025 déc 24]. page 160-3.Available from: https://ieeexplore.ieee.org/document/9105156/
17. Kupidura P, Kępa A, Krawczyk P. Comparative analysis of the performance of selected machine learning algorithms depending on the size of the training sample. Rep. Geod. Geoinformatics 2024;118:20240015.
18. Stefanus K, Leong H. COMPARISON OF RANDOM FOREST ALGORITHM ACCURACY WITH XGBOOST USING HYPERPARAMETERS. Proxies J. Inform. 2024;7:15-23.
19. Simou MR, Houran N, Benayad M, Maanan M, Loulad S, Rhinane H. MONITORING FOREST DEGRADATION OVER FOUR DECADES USING REMOTE SENSING AND MACHINE LEARNING CLASSIFICATION ALGORITHMS IN BOUSKOURA, MOROCCO. Int. Arch. Photogramm. Remote Sens. Spat. Inf. Sci. 2024;XLVIII-4/W9-2024:337-42.
20. Barakat A, Brhaiberh M, Ettaqy A, El Jazouli A, Ennaji W. Machine learning based forest species susceptibility mapping using Sentinel 2A data and GIS: A case study of Ait Bouzid forest (Central High Atlas, Morocco). Bull. Geogr. Phys. Geogr. Ser. 2023;63-78.
21. Alibakhshi S. A robust approach and analytical tool for identifying early warning signals of forest mortality. Ecol. Indic. 2023;155:110983.
22. Arar A, Nouidjem Y, Bounar R, Tabet S, Kouba Y. Modeling of the current and future potential distribution of Atlas cedar (Cedrus atlantica) forests revealed shifts in the latitudinal, longitudinal and altitudinal range towards more humid conditions. Ecol. Quest. 2020;31:49.
23. Linares JC, Taïqui L, Camarero JJ. Increasing Drought Sensitivity and Decline of Atlas Cedar (Cedrus atlantica) in the Moroccan Middle Atlas Forests. Forests 2011;2:777-96.
24. Jurado J, Ramos M, Enríquez C, Feito F. The Impact of Canopy Reflectance on the 3D Structure of Individual Trees in a Mediterranean Forest. Remote Sens. 2020;12:1430.
25. Coudel M, Aubert P, Aderghal M, Hély C. Pastoral and woodcutting activities drive *Cedrus atlantica* Mediterranean forest structure in the Moroccan Middle Atlas. Ecol. Appl. 2016;26:574-86.
26. Coudel M, Aubert P, Aderghal M, Hély C. Pastoral and woodcutting activities drive *Cedrus atlantica* Mediterranean forest structure in the Moroccan Middle Atlas. Ecol. Appl. 2016;26:574-86.
27. Bonannella C. Spatiotemporal modeling of vegetation dynamics in a changing environment: combining earth observation and machine learning [Internet]. 2024 [cité 2025 déc 24];Available from: https://research.wur.nl/en/publications/bca0991e-20ab-4c38-b91b-6eded1de8b3a
28. Williams T, Martinuzzi F, Camps-Valls G, D. Mahecha M. Evaluating Forest Resilience in Europe with Deep Learning Persistence Analysis [Internet]. 2025 [cité 2025 déc 24];Available from: https://meetingorganizer.copernicus.org/EGU24/EGU24-20805.html
29. Hammi S, Simonneaux V, Cordier JB, Genin D, Alifriqui M, Montes N, et al. Can traditional forest management buffer forest depletion? Dynamics of Moroccan High Atlas Mountain forests using remote sensing and vegetation analysis. For. Ecol. Manag. 2010;260:1861-72.
30. Linares JC, Pazo Sarria R, Taïqui L, Camarero JJ, Ochoa V, Lechuga V, et al. Efectos de las tendencias climáticas y la degradación del hábitat sobre el decaimiento de los cedrales (Cedrus atlantica) del norte de Marruecos. Ecosistemas 2012;21:7-14.
31. Moukrim S, Lahssini S, Rifai N, Menzou K, Mharzi-Alaoui H, Labbaci A, et al. Modélisation de la distribution potentielle de Cedrus atlantica Manetti au Maroc et impacts du changement climatique. BOIS FORETS Trop. 2020;344:3-16.
32. Seddouki M, Benayad M, Aamir Z, Tahiri M, Maanan M, Rhinane H. USING MACHINE LEARNING COUPLED WITH REMOTE SENSING FOR FOREST FIRE SUSCEPTIBILITY MAPPING. CASE STUDY TETOUAN PROVINCE, NORTHERN MOROCCO. Int. Arch. Photogramm. Remote Sens. Spat. Inf. Sci. 2023;XLVIII-4/W6-2022:333-42.
33. Dietenberger S, Mueller MM, Adam M, Bachmann F, Stöcker B, Hese S, et al. Digital Forest Inventory Based on UAV Imagery [Internet]. In: IGARSS 2024 - 2024 IEEE International Geoscience and Remote Sensing

Symposium. Athens, Greece: IEEE; 2024 [cité 2025 déc 24]. page 4439-42.Available from: https://ieeexplore.ieee.org/document/10641040/
34. Kukunda CB, Beckschäfer P, Magdon P, Schall P, Wirth C, Kleinn C. Scale-guided mapping of forest stand structural heterogeneity from airborne LiDAR. Ecol. Indic. 2019;102:410-25.